

The Dynamics of Subhalos in Warm Dark Matter Models

Alexander Knebe¹, Bastian Arnold^{1,2}, Chris Power³, & Brad K. Gibson^{4,5}

¹*Astrophysikalisches Institut Potsdam, An der Sternwarte 16, 14482 Potsdam, Germany*

²*Institut für Astronomie, Universität Wien, Türkenschanze 17, 1180 Wien, Austria*

³*Centre for Astrophysics & Supercomputing, Swinburne University, Mail H39, Hawthorn VIC 3122, Australia*

⁴*Centre for Astrophysics, University of Central Lancashire, Preston PR1 2HE, UK*

⁵*School of Physics, University of Sydney, NSW 2006, Australia*

14 October 2021

ABSTRACT

We present a comparison of the properties of substructure halos (*subhalos*) orbiting within host halos that form in Cold Dark Matter (CDM) and Warm Dark Matter (WDM) cosmologies. Our study focuses on selected properties of these subhalos, namely their anisotropic spatial distribution within the hosts; the existence of a “backsplash” population; the age-distance relation; the degree to which they suffer mass loss; and the distribution of relative (infall) velocities with respect to the hosts. We find that the number density of subhalos in our WDM model is suppressed relative to that in the CDM model, as we would expect. Interestingly, our analysis reveals that backsplash subhalos exist in both the WDM and CDM models. Indeed, there are no statistically significant differences between the spatial distributions of subhalos in the CDM and WDM models. There is evidence that subhalos in the WDM model suffer enhanced mass loss relative to their counterparts in the CDM model, reflecting their lower central densities. We note also a tendency for the (infall) velocities of subhalos in the WDM model to be higher than in the CDM model. Nevertheless, we conclude that observational tests based on either the spatial distribution or the kinematics of the subhalo population are unlikely to help us to differentiate between the CDM model and our adopted WDM model.

Key words: methods: n-body simulations – galaxies: halos – galaxies: evolution – cosmology: theory – dark matter

1 INTRODUCTION

The currently favoured Λ CDM model of cosmological structure formation has proven to be extremely successful at describing the clustering of matter on intermediate to large scales (e.g., Springel et al. 2005; Spergel 2007). In contrast, it has been argued that the predictions of the Λ CDM model are at odds with observations on the scales of galaxies, on the basis of cosmological N -body simulations. Cold Dark Matter (CDM) halos are predicted to have “cuspy” density profiles with inner logarithmic slopes of approximately -1.2 (e.g., Navarro et al. 2004; Tasitsiomi et al. 2004; Diemand et al. 2005; Reed et al. 2005), whereas high resolution observations of low surface brightness galaxies appear to require halos with constant density cores (e.g., Gentile et al. 2007; McGaugh et al. 2007). Furthermore, CDM halos are predicted to contain a wealth of substructure, which we might expect to observe as satellite galaxies within galactic halos, in sharp contrast to the observed abundance of satellites around our Galaxy and others (Klypin et al. 1999; Moore et al. 1999).

Suggested solutions to these problems have included allowing the dark matter to be collisional (i.e. *self-interacting*) rather than collisionless (Spergel & Steinhardt 2000; Bento et al. 2000), allowing it to be warm rather than cold (Bode et al. 2001;

Avila-Reese et al. 2001; Knebe et al. 2002), and introducing non-standard modifications to an otherwise unperturbed CDM power spectrum (e.g., Bullock 2001; Little et al. 2003). Arguably the most promising (and least intrusive) modification to the dark matter paradigm is to allow the dark matter particle to be warm. In such a case, warm dark matter particles will have a relatively high thermal velocity dispersion at decoupling and therefore a non-negligible *free-streaming scale* λ_{fs} . This modification results in a change to the primordial matter power spectrum, corresponding to a damping of density perturbations on scales below a *filtering scale* R_f (which is related to the free-streaming scale λ_{fs}), which in turn is related to a filtering mass M_f (Bardeen et al. 1986; Bode et al. 2001; Avila-Reese et al. 2001; Knebe et al. 2002).

Previous studies have revealed that WDM can resolve some of the tension between theoretical prediction and observation. In particular, the abundance of substructure halos (hereafter subhalos) is greatly reduced in WDM models (Bode et al. 2001; Avila-Reese et al. 2001; Knebe et al. 2002) compared to the CDM model. However, the simulations used in these studies did not have sufficient resolution to follow the orbits of subhalos in detail, and so these

arXiv:0802.1628v1 [astro-ph] 12 Feb 2008

results are based on a snapshot of the subhalo population, static in time rather than a dynamic entity.

Over the last decade cosmological N -body simulations have advanced and reached a stage where it is possible to study the dynamics of well resolved subhalos and satellite galaxies and use them as a probe of cosmology. This field – dubbed “near-field cosmology” (e.g., Bland-Hawthorn & Peebles 2006) – has prompted numerous studies (e.g., Warnick et al. 2008; Colin et al. 2007; Sales et al. 2007; Faltenbacher et al. 2007; Diemand et al. 2007; Libeskind et al. 2007; Kang et al. 2007; Warnick & Knebe 2006; Agustsson & Brainerd 2006; Knebe et al. 2006; Libeskind et al. 2005; Reed et al. 2005; De Lucia et al. 2004; Gao et al. 2004; Gill et al. 2004; Knebe et al. 2004; Kravtsov et al. 2004; Zentner & Bullock 2003), but as yet there have been no in-depth comparisons of subhalos in CDM and WDM models. We address this in the present study, using high resolution resimulations of a set of “identical” galaxy clusters (see next section) forming in CDM and WDM models to compare and contrast properties of their subhalo populations.

Rather than seeking to reproduce and verify all of the recent results for subhalos derived from simulations of the CDM model, we focus on selected properties of the subhalo population. Namely, we set out to validate the existence of the so-called “backsplash” population reported in Gill et al. (2005) (see also Mamon et al. 2004; Moore et al. 2004; Balogh et al. 2000), the anisotropic spatial distribution of satellites (e.g., Bailin et al. 2007; Agustsson & Brainerd 2006; Zentner et al. 2005; Libeskind et al. 2005; Knebe et al. 2004), the putative age-distance relation (cf., Gao et al. 2004; Moore et al. 2004), and the degree to which subhalos suffer mass loss. We also examine the relative velocities of subhalos with respect to their hosts. This is of particular interest because it has been argued that the collision velocity of the “Bullet Cluster” (Milosavljević et al. 2007; Markevitch et al. 2002) may pose another challenge to CDM (e.g., Springel & Farrar 2007; Hayashi & White 2006). While it might be expected that the large scale tidal field will be more important for collision velocities in mergers, it is nevertheless interesting to see whether the precise nature of the dark matter might play a role. Having characterised these properties, we can quantitatively address the question of whether or not the spatial and kinematic properties of subhalos at the present day could be used to differentiate between the CDM and WDM models.

2 THE NUMERICAL SIMULATIONS

2.1 The Raw Data

Our analysis is based on suite of high-resolution N -body simulations. They were carried out using the publicly available adaptive mesh refinement code `MLAPM` (Knebe et al. 2001) focusing on the formation and evolution of dark matter galaxy clusters containing of order one million particles, with mass resolution $1.6 \times 10^8 h^{-1} M_\odot$ and force resolution $\sim 2h^{-1}$ kpc. We first created a set of four independent initial conditions at redshift $z = 45$ in a standard Λ CDM cosmology ($\Omega_0 = 0.3, \Omega_\lambda = 0.7, \Omega_b = 0.04, h = 0.7, \sigma_8 = 0.9$). 512^3 particles were placed in a box of side length $64h^{-1}$ Mpc giving a mass resolution of $m_p = 1.6 \times 10^8 h^{-1} M_\odot$. For each of these initial conditions we iteratively collapsed eight adjacent particles to one particle reducing our particle number to 128^3 particles. These lower mass resolution initial conditions were then evolved until $z = 0$. Then, as described by Tormen (1997), for each cluster the particles within five times the virial radius were tracked back to their Lagrangian positions at the initial redshift ($z = 45$). Those

particles were then regenerated to their original mass resolution and positions, with the next layer of surrounding large particles regenerated only to one level (i.e. 8 times the original mass resolution), and the remaining particles were left 64 times more massive than the particles resident with the host cluster. This conservative criterion was selected in order to minimise contamination of the final high-resolution halos with massive particles.

The three warm dark matter halos were simulated using the same techniques. In fact, the only difference between the CDM and WDM halos is the functional form of the primordial power spectrum used as an input for the initial conditions generator. We follow Bardeen et al. (1986) and modify the CDM power spectrum by multiplying it with a damping function $F_{\text{WDM}}^2(k)$, where

$$F_{\text{WDM}}(k) = \exp \left[-\frac{kR_d}{2} - \frac{(kR_d)^2}{2} \right]. \quad (1)$$

Following Bardeen et al. (1986), we parameterise the damping scale R_d in terms of the warmon density parameter Ω_{wdm} , its mass m_{wdm} and the dimensionless Hubble parameter h ,

$$R_d \simeq 0.074 \left(\frac{m_{\text{wdm}}}{\text{keV}} \right)^{-4/3} \left(\frac{\Omega_{\text{wdm}}}{0.3} \right)^{1/3} \left(\frac{h}{0.7} \right)^{5/3} h^{-1} \text{Mpc}. \quad (2)$$

We adopt a warmon mass of $m_{\text{wdm}} = 0.5$ keV, which gives a damping scale of $R_d = 0.186h^{-1}$ Mpc. The filtering scale R_f can be obtained by determining the wavenumber of the mode at which the amplitude of the linear density fluctuation is suppressed by a factor of two, and then computing half the comoving wavelength. It is straightforward to evaluate this from the WDM and CDM power spectra. For our choice of warmon mass and cosmological parameters, we find that this wavenumber corresponds to $k = 2.553 h \text{Mpc}^{-1}$ and therefore the filtering scale (mass) is $R_f = 1.24 h^{-1} \text{Mpc}$ ($M_f = 6.653 \times 10^{11} h^{-1} M_\odot$).

Note that our choice of warmon mass is lower than recent lower limits derived from combined analysis of observed properties of the matter power spectrum as inferred from the Sloan Digital Sky Survey Lyman- α flux power spectrum, cosmic microwave background data and the galaxy power spectrum, which vary between, e.g., $m_{\text{wdm}} \geq 3$ keV (Abazajian 2006) and $m_{\text{wdm}} \geq 10$ keV (Viel et al. 2006). However, it is consistent with published estimates of the ~ 0.5 keV warmon mass that would resolve the “overabundance” of dark matter substructure in galactic halos (e.g. Moore et al. 1999; Dalcanton & Hogan 2001; Goerdt et al. 2006). By focusing on the lowest warmon mass that could be considered consistent with observational data, we can explore subhalo dynamics in a plausible model, yet one in which the effects of the warmon should be more pronounced and therefore easier to identify when comparing and contrasting with the CDM model.

We note that the three CDM halos CDM1, CDM2, and CDM3 have appeared previously in both Warnick & Knebe (2006) and Warnick et al. (2008), in which they corresponded to the “C3”, “C7” and “C8” systems.

2.2 Discreteness Effects

It has been argued in the recent study of Wang & White (2007) that WDM halos below a given fraction of the filtering mass M_f are spurious, arising from the unphysical fragmentation of filaments. They provided the following expression (based upon simulations of the Hot Dark Matter model)

$$M_{\text{lim}} \simeq 10.1 \bar{\rho} d k_{\text{peak}}^{-2}. \quad (3)$$

$\bar{\rho}$ is the mean density, d is the mean interparticle separation, and k_{peak} is the wavenumber at which $\Delta^2(k) = k^3 P(k)$ reaches its maximum.

We have taken care to compute M_{lim} , noting that our simulations use boxes of side $64h^{-1}\text{Mpc}$, an effective number of particles 512^3 , a density parameter of $\Omega_0=0.3$ and a peak wavenumber of $k_{\text{peak}}=1.78 h \text{ Mpc}^{-1}$. These numbers give $d=0.125 h^{-1}\text{Mpc}$, $\bar{\rho}=8.3265 h^2 M_{\odot} \text{ Mpc}^{-3}$ and so $M_{\text{lim}}=3.317828 \times 10^{10} h^{-1} M_{\odot}$. Our particle mass is $m_p = 1.626269 \times 10^8 h^{-1} M_{\odot}$, and so we find that M_{lim} is equivalent to 204 particles. Therefore, this corresponds to the mass cut applied in the following analysis.

We have also applied a cut of $2M_{\text{lim}}$ to our data and checked our results to ensure that they are unaffected by spurious halos. This reveals that our results remain unchanged and therefore are stable. We do not find any systematic biases in our data if we employ mass cuts of M_{lim} or $2M_{\text{lim}}$. We have looked for trends in our data that we would expect to be present if they were affected by spurious haloes (such as the distribution of concentrations) but we find no obvious signatures. Therefore we conclude that our results are robust and unaffected by particle discreteness.

2.3 The Halos

Both the halos and their subhalos are identified using AHF¹, a modification of the MHF² algorithm presented in Gill et al. (2004), which has been parallelised using the MPI (Message Passing Interface) libraries. AHF utilises the adaptive grid hierarchy of MLAPM to locate (sub)halos as peaks in an adaptively smoothed density field. Local potential minima are computed for each peak and the set of particles that are gravitationally bound to the peak are returned. If the peak contains in excess of 20 particles, then it is considered a (sub)halo and it is retained for further analysis.

For each (sub)halo we calculate a suite of canonical properties from particles within the virial/truncation radius. We define the virial radius R_{vir} as the point at which the density profile (measured in terms of the cosmological background density ρ_b) drops below the virial overdensity Δ_{vir} , i.e. $M(< R_{\text{vir}})/(4\pi R_{\text{vir}}^3/3) = \Delta_{\text{vir}}\rho_b$. Here ρ_b is the mean density of the background (Universe). Following convention, we assume the cosmology- and redshift-dependent definition of Δ_{vir} ; for a distinct (i.e. host) halo in a ΛCDM cosmology with the cosmological parameters that we have adopted, $\Delta_{\text{vir}} = 340$ at $z = 0$. This prescription is not appropriate for subhalos in the dense environs of their host halo, where the local density exceeds $\Delta_{\text{vir}}\rho_b$, and so the density profile will show a characteristic upturn at a radius $R \lesssim R_{\text{vir}}$. In this case we use the radius at which the density profile shows this upturn to define the truncation radius for the subhalo. Further details of this approach (and especially the ‘‘halo tracking’’ used to obtain the temporal evolution of subhalos) can be found in Gill et al. (2004).

In Table 1 we summarise some of the properties of the host halos along with particulars of their respective subhalo populations.

* The peak value $k_{\text{peak}}=1.78 h \text{ Mpc}^{-1}$ has been determined numerically from the (tabulated) warm dark matter power spectrum used in this study based upon a CDM power spectrum calculated with the publically available CMBFAST code (Seljak & Zaldarriaga 1996) and modified according to Eq. (1).

¹ AMIGA’s-Halo-Finder; AHF can be downloaded from <http://www.aip.de/People/aknebe/AMIGA>. AMIGA is the successor to MLAPM.

² MLAPM’s-Halo-Finder

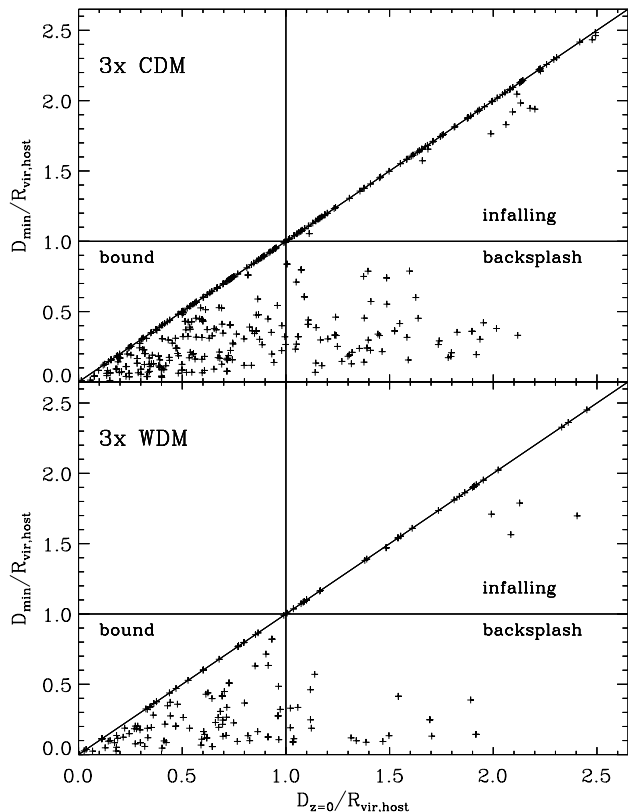


Figure 1. Minimum distance as a function of present-day distance.

3 ANALYSIS OF THE SUBHALO POPULATION

3.1 The ‘‘Backsplash’’ Population

It has been noted that a significant population of halos on the outskirts of present-day galaxy- and cluster-mass host halos once resided within the virial radii of these hosts at earlier times (Warnick et al. 2008; Gill et al. 2005; Mamon et al. 2004; Moore et al. 2004; Balogh et al. 2000). These results are based on simulations of the CDM model, but it is interesting to ask whether such a ‘‘backsplash’’ population exists in the WDM model. We expect there to be fewer satellites in WDM models and these satellites will tend to have lower concentrations (Knebe et al. 2002; Avila-Reese et al. 2001; Bode et al. 2001), which, when combined, should affect the numbers of ‘‘backsplash’’ halos. The lower the concentration of a (sub)halo, the greater the likelihood that it will be tidally disrupted within the host. Therefore, we might expect the numbers of backsplash halos to be suppressed in WDM models.

In Figure 1 we plot the minimum halocentric distance reached by a (sub)halo against its present day halocentric radius. Note that we combine data for all three halos in the CDM and WDM models respectively. As expected, backsplash halos are present in both the CDM and WDM models, although the numbers are reduced in the WDM model. Table 1 reveals that the youngest system (i.e. host #3) has the smallest fraction of backsplash halos; this reflects the fact that this system has experienced a recent triple merger (cf. Warnick et al. 2008; Warnick & Knebe 2006). Interestingly, we find again (cf. Gill et al. 2005) that the number of infalling halos is of the same order as the number of backsplash halos in both the CDM and WDM models.

Table 1. Summary of the host halos properties and their subhalo populations. The age is given in Gyrs, R_{vir} is measured in h^{-1} kpc, masses in $10^{14} h^{-1} M_{\odot}$ and the velocity dispersion σ_v in km/sec. We follow Lacey & Cole (1993) and define the formation redshift of our host halos as the redshift at which the halo’s most massive progenitor first contains in excess of half its present day mass. The concentration $c_{1/5} = R_{\text{vir}}/R_{1/5}$ is defined via the radius $R_{1/5}$ that encompasses $1/5^{\text{th}}$ of the virial mass. Shape is quantified by the triaxiality parameter $T = (a^2 - b^2)/(a^2 - c^2)$ and the eigenvalues of the inertia tensor $a > b > c$. N_{sat}^X measures the number of a certain subset X (int=interior, inf=infalling, back=backsplash) of subhalos while $N_{\text{sat}}^{<2.5R_{\text{vir}}}$ gives the total number of subhalos within $2.5R_{\text{vir}}$; note that these numbers only reflect subhaloes in excess of 200 particles.

model	z_{form}	age	R_{vir}	M_{vir}	σ_v	$c_{1/5}$	T	b/a	c/a	$\max\{M_{\text{sat}}\}$	$N_{\text{sat}}^{<2.5R_{\text{vir}}}$	$N_{\text{sat}}^{\text{int}}$	$N_{\text{sat}}^{\text{inf}}$	$N_{\text{sat}}^{\text{back}}$
CDM1	0.805	6.9	973	1.1	833	6.57	0.952	0.749	0.212	0.12	54	26	13	15
CDM2	0.443	4.6	1347	2.9	1185	5.91	0.836	0.597	0.467	0.18	182	91	53	38
CDM3	0.237	2.8	1379	3.1	1092	5.84	0.867	0.818	0.749	0.49	159	126	31	2
WDM1	0.871	7.1	967	1.1	783	5.98	0.958	0.773	0.206	0.09	17	6	7	4
WDM2	0.643	5.9	1340	2.8	1093	6.09	0.887	0.705	0.423	0.45	77	52	16	9
WDM3	0.284	3.2	1352	3.0	1119	3.69	0.837	0.693	0.576	0.36	68	50	12	6

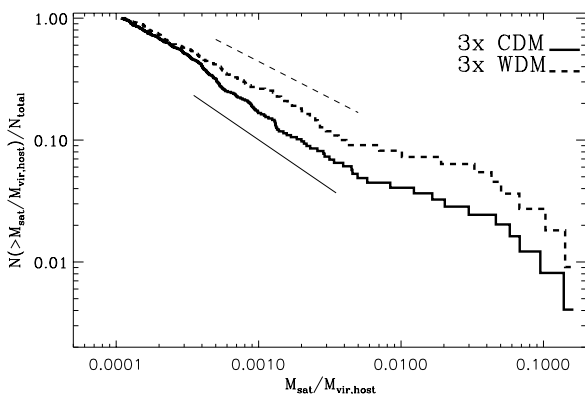


Figure 2. The cumulative distribution of all interior subhalos normalised to the total number of satellites. The short thin lines represent curves with the logarithmic slopes of $\alpha = -0.8$ (solid) and $\alpha = -0.6$ (dashed), respectively.

3.2 Mass Spectra

The mass spectrum of satellite galaxies in WDM and CDM has been studied previously (Knebe et al. 2002; Avila-Reese et al. 2001; Bode et al. 2001), but we consider it here briefly for completeness. In Figure 2 we show the cumulative mass functions of subhalos normalised to the total number of subhalos, where we normalise the subhalo mass by the host halo mass. It is readily apparent that the abundance of low-mass halos is suppressed in WDM cosmologies. We fit a power-law to this mass function,

$$\frac{N(>M)}{N_{\text{total,interior}}} \propto \left(\frac{M_{\text{sat}}}{M_{\text{vir,host}}}\right)^{\alpha}, \quad (4)$$

and obtain logarithmic slopes of $\alpha = -0.8$ for CDM and $\alpha = -0.6$ for WDM. This is consistent with the findings of previous studies for CDM subhalos (e.g., Shaw et al. 2007; Reed et al. 2005; Gill et al. 2004; De Lucia et al. 2004; Gao et al. 2004).

We also calculate the mass functions of the infalling and back-splash halo populations, which we show in Figure 3. We observe a general trend that back-splash halos contain fewer high-mass objects in comparison to the infalling halos. This reflects the importance of tidally induced mass loss for back-splash halos, which we quantify in the next section (cf. also Warnick et al. 2008).

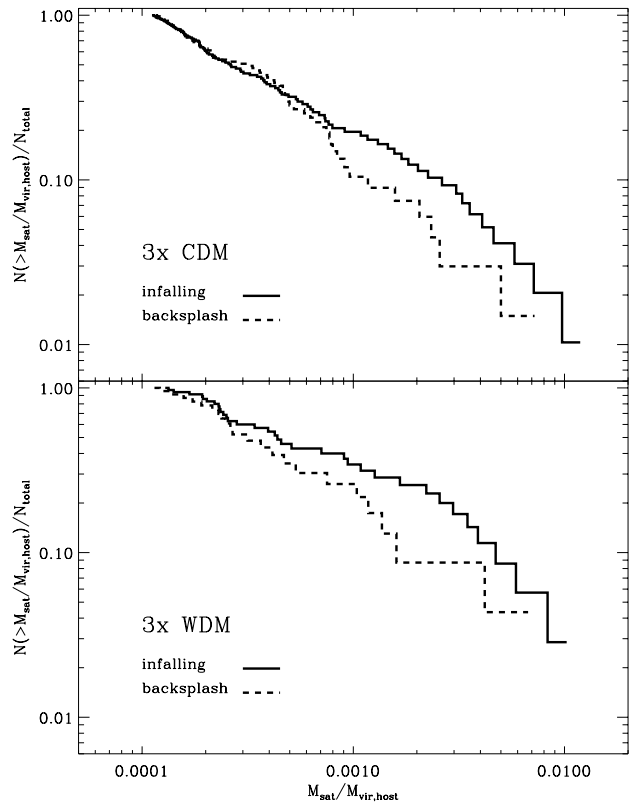


Figure 3. As in Figure 2 but for the infalling and back-splash populations respectively.

3.3 Mass Loss

There is a general consensus that subhalos in WDM models are less concentrated than their counterparts in CDM models (Knebe et al. 2002; Bode et al. 2001; Avila-Reese et al. 2001) and therefore more susceptible to tidal destruction while orbiting within the dense environs of their host halo. We verify this in Figure 4 and Figure 5 where we plot the total (fractional) mass loss as a function of distance to the host for both the interior and the back-splash population. The mass loss is measured over the time period from infall onto the host (i.e. the first time a satellite crosses the virial radius of the host on an inward trajectory) until the present-day.

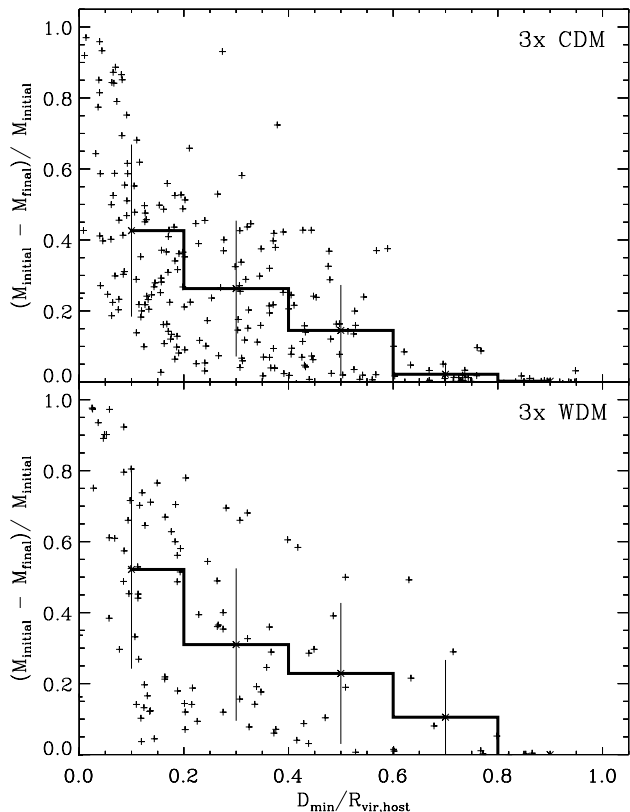


Figure 4. The total (fractional) mass loss of interior subhalos as a function of minimum distance to the host. The error bars represent the standard deviation.

In both dark matter models the average mass loss (presented as histograms in Figure 4) is a monotonic decreasing function of minimum distance. However, in the WDM model this function is pointwise greater than the corresponding curve in CDM, which would be expected if mass loss is enhanced as a result of the lower concentrations of subhalos in the WDM model.

Surprisingly, the relation between mass loss and minimum distance is not as steep for backplash halos as for interior subhalos (Figure 5). Nevertheless, (sub)halos plunging deeper into the potential well of the host experience greater mass loss – as expected and confirmed for the interior population (e.g., Sales et al. 2007; Diemand et al. 2007; Kravtsov et al. 2004; Gao et al. 2004). On average, backplash halos in the WDM model suffer greater mass loss than their CDM counterparts.

3.4 Spatial Anisotropy

There is good reason to believe that the spatial distribution of subhalos (and the subset corresponding to satellite galaxies) in both cluster sized systems and galactic halos is anisotropic in the CDM model (e.g., Faltenbacher et al. 2007; Kang et al. 2007; Libeskind et al. 2007; Agustsson & Brainerd 2007, 2006; Zentner et al. 2005; Libeskind et al. 2005; Knebe et al. 2004), and so it is interesting to ask whether the same can be said of the WDM model.

For each of our host halos, we compute the cumulative fraction of subhalos which have cosine of the angle

$$\cos \Phi = \mathbf{R}_{\text{sat},z=0} \cdot \mathbf{E}_1; \quad (5)$$

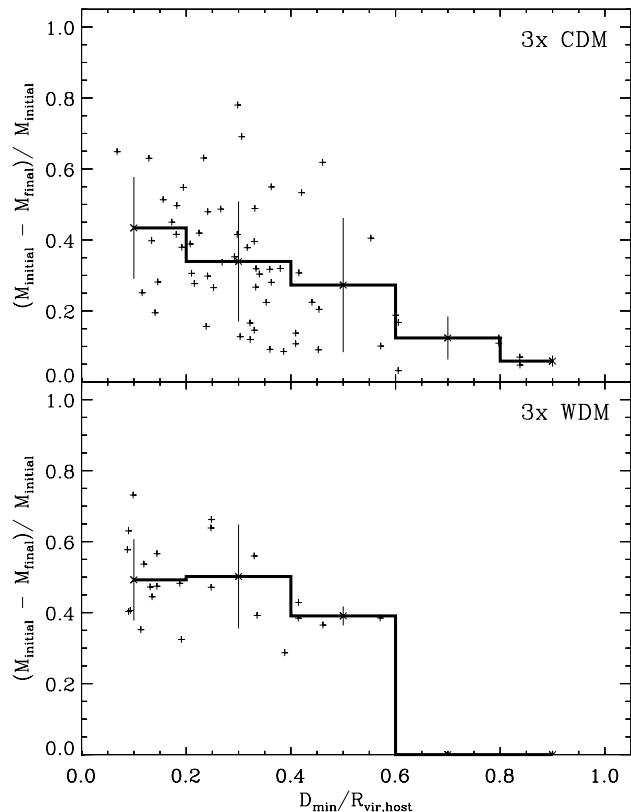


Figure 5. Same as Figure 4 but for the backplash population.

this measures the position of a subhalo relative to the host $\mathbf{R}_{\text{sat},z=0}$ and the host’s major axis \mathbf{E}_1 . The host’s major axis is identified using the eigenvalues and eigenvectors of its moment of inertia tensor, where the eigenvector corresponding to the smallest eigenvalue defines the major axis.

The resulting distributions of $\cos \Phi$ are shown in Figure 6 for subhalos within the host’s virial radius, which confirms that the spatial anisotropy is present in the WDM model although not as pronounced as for the CDM case. Although we do not show the result here as it (probably) lies below the credibility level of the WDM simulation (Wang & White 2007), we note that very low mass systems (i.e. $M_{\text{sat}} < 10^{-4} M_{\text{host}}$) correlate more strongly with the major axis than the remainder of the satellites – for both dark matter models. This is consistent with the expectation that (especially low mass) objects are primarily channelled along the filaments feeding the cluster (cf. also Knebe et al. 2004). The thin dashed line represents an isotropic distribution or the “uniform continuous distribution function” (UCDF).

We have computed the same distribution for both the backplash and infalling satellites in Figure 7. Interestingly we find that the spatial anisotropy is even stronger for the backplash population than for the interior objects even though it is skewed towards $\cos \Phi \approx 0.55$ for the WDM model and hence no perfect alignment with \mathbf{E}_1 anymore (but nevertheless an anisotropic distribution). One possible explanation for this could be that backplash halos tend to be on radial orbits that are either plunging through the host or grazing the “virial surface”. If this is the case, we might expect to observe a tendency for the infalling population to align with the major axis as verified in the lower panel of Figure 7. In addition

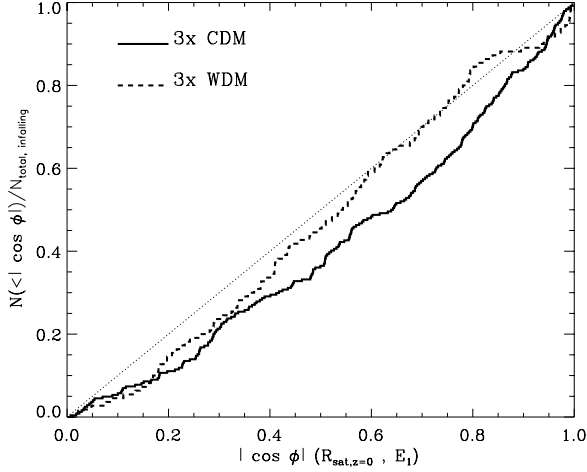


Figure 6. Cumulative fraction of satellites with the absolute value of the cosine of the zenith angle $<|\cos \phi|$. The zenith angle, $0 < \phi < \pi$, is defined as the angle from the major axis of the dark matter distribution of the host. The dotted line corresponds to an isotropic distribution or the “uniform continuous distribution function”.

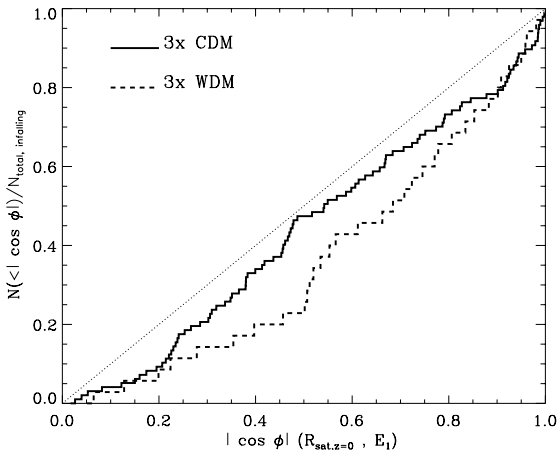
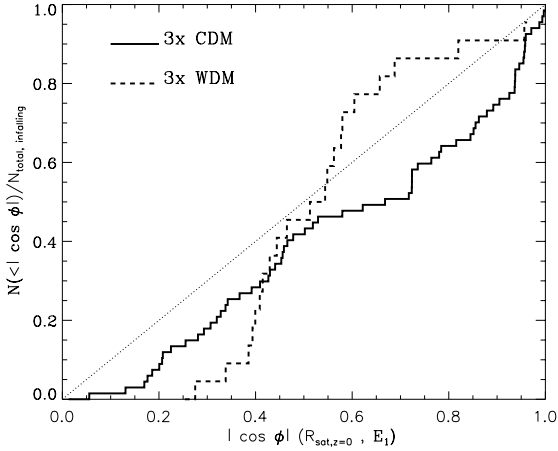


Figure 7. Same as Figure 6 but for the backplash (upper panel) and infalling (lower panel) population, respectively.

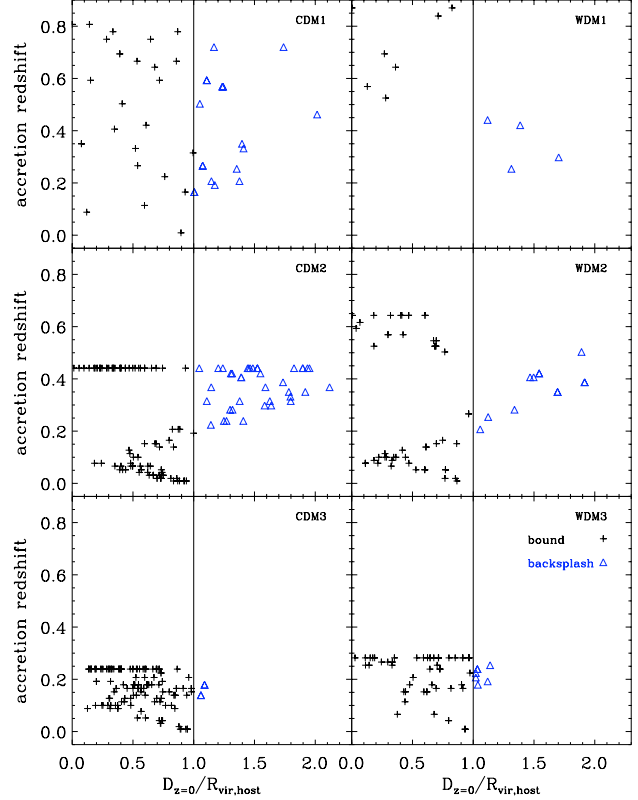


Figure 8. Age-Distance Relation. We define the “age” of a subhalo as the period of time that has elapsed since it first crossed the virial radius of its host on an inward trajectory. The redshift at which this occurs is the “accretion redshift”. $D_{z=0}/R_{\text{vir,host}}$ measures the subhalo’s current distance to with respects to the centre of the host. For clarity, the triangles represent backplash halos while black crosses denote “interior” subhalos.

we note that the infalling WDM satellites show a more pronounced tendency to be aligned with the major axis of the respective host. This goes along with the expectation for (sub)haloes to be concentrated in the filaments and channelled along them into the cluster (e.g., Knebe et al. 2004).

3.5 Age-Distance Relation

Is there is a correlation between the infall time of a satellite and its present-day halocentric radius? Previous studies using cosmological simulations have argued that “older” subhalos tend to lie closer to the centre of the host (Willman et al. 2004; Gao et al. 2004), but there are also claims to the contrary (Moore et al. 2004). Here the age of a subhalo corresponds to the period of time that has elapsed since it was first accreted by the host (accretion redshift), entering the virial radius on an inward trajectory.

We investigate whether such a correlation between a subhalo’s age or *accretion redshift* and halocentric radius exists in our data in Figure 8. Crosses represent “interior” subhalos within the virial radius at the present day while triangles represent backplash halos. Because we output our snapshots at discrete intervals, the times at which subhalos are accreted appear discrete. It is possible to correct for this discreteness by interpolating the growth of the virial radius and the positions of subhalos between snapshots, but we output

snapshots sufficiently frequently to make the uncertainty introduced by discreteness negligible.

Figure 8 reveals that the correlation between radius and age is not a straightforward one. The CDM1/WDM1 system is hard to interpret because there is no strong trend for subhalos within the virial radius. However, there are interesting trends in the CDM2/WDM2 and CDM3/WDM3 that suggest that there may be distinct populations following distinct age-distance relations. The most recently accreted subhalos, with accretion redshifts $z \lesssim 0.1$, show the expected trend for accretion redshift to increase with decreasing redshift. However, subhalos accreted at $z \gtrsim 0.1$ appear to follow an inverse relation, tending to have higher accretion redshifts for larger halocentric radii, and this trend continues beyond the virial radius into the backsplash population. Finally, we note that the “oldest” subhalos do not appear to follow any trend, instead forming a hard upper edge in each panel. However, this edge is an artifact of our method for tracking subhalos (cf. Gill et al. 2004) and corresponds to the formation redshift, z_{form} , of the respective host halo. This explains why there is a systematic shift to higher redshifts from the lower plot to the upper one – our halo tracker starts following subhalos at z_{form} and so it cannot “see” (sub)halos prior to z_{form} . Therefore all subhalos that resided within the host at this initial time appear as infalling ones.

This figure also reveals that no backsplash halos have been accreted more recently than $z \approx 0.15$, which corresponds to a period of ~ 2 billion years. This might be considered the minimum time a backsplash halo spends within the virial radius of the host halo. We can compare this to the time scale t_{dyn} for a subhalo to complete one circular orbit at the virial radius;

$$t_{\text{dyn}} = \sqrt{\frac{3\pi}{G\rho}} \approx \sqrt{\frac{3\pi}{G\Delta_{\text{vir}}\rho_{\text{b}}}} \rho_{\text{b}}^{-1/2}, \quad (6)$$

where we used $\rho \approx \Delta_{\text{vir}}\rho_{\text{b}}$. This leads to $t_{\text{dyn}} \approx 6 \times 10^9$ yr. Therefore, the minimum time t_{inside} a subhalo spends inside its host is approximately $1/3^{\text{rd}}$ the time it would take to complete one orbit at the virial radius. This suggests that backsplash haloes are on preferentially radial orbits, and explains why subhalos accreted at earlier times are preferably found outside R_{vir} today.

We conclude that an age-distance relation akin to the one reported by Gao et al. (2004) is valid only for “recently” accreted subhalos. According to Figure 8, there is a clear correlation between a subhalo’s age and its distance apparent in CDM2/WDM2 and CDM3/WDM3, the two youngest sets of hosts in our sample, and this correlation is apparent for objects accreted after $z = 0.2$. However, as we note above, there is some evidence that there may be distinct subhalo populations, separated according to their accretion redshift, that follow distinct relations and inverse relations.

It is worth noting that Gao et al. (2004) observed an age-distance relation over a much greater time span ranging from $z \sim 0.9$ down to $z \sim 0.3 - 0.4$. These authors identify all subhalos at $z=1$ and track them forward in time, which is equivalent to our approach (we start tracking subhalos at the formation redshift of the host, which varies between $z \simeq 0.8$ for CDM1/WDM1 to $z \simeq 0.2$ for CDM3/WDM3). We note that accretion in their data appears to be complete by $z \sim 0.3$ (see upper panel of their Figure 15). However, it remains unclear why there is no further accretion apparent in that plot for smaller redshifts as the fraction of accreted subhalos increases at least down to $z \sim 0.1$ (cf. upper left panel in their Figure 12). Moore et al. (2004) deduced from their analysis that any age-distance relation present in their data had to be very weak with

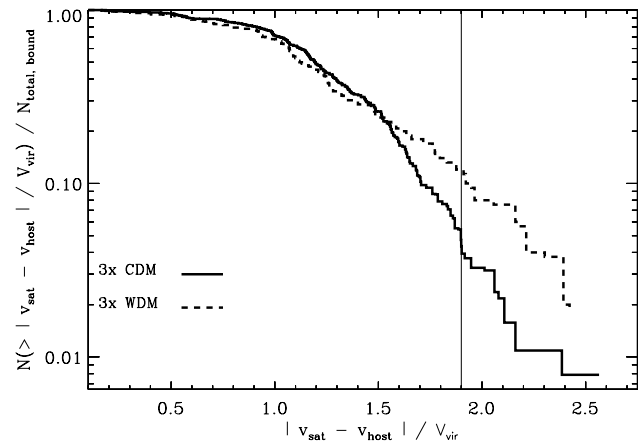


Figure 9. Cumulative distribution of relative velocity between all interior subhalos and their respective host. The thin vertical line is representative of the collisional speed of the “Bullet” cluster.

a large scatter. We note that these authors identify subhalos at $z=0$ and track their merger trees backwards in time.

It is clear from our analysis that any conclusions we draw must be tentative – if we are to gain greater insight into the age-distance relation then we must draw upon a larger (i.e. statistical) sample of host halos. Nevertheless we note that any age-distance relation is apparent in the subhalo populations in both the CDM and WDM models.

It is notable that there are no counterparts in the WDM1 system to the “old” backsplash population we observe in the CDM1 model. To better understand why this might so, we checked the distribution of infall velocities for subhalos that were accreted at early times in each of host (i.e. $z > 0.75$ for CDM1 and $z > 0.80$ for WDM1). We found that the typical subhalo velocity in the CDM1 run was approximately 30% larger than in the WDM1 run. This explains why we do not find an “old” backsplash population in the WDM1 run – the typical infall velocity of a subhalo is too low to allow it to escape the host and become a backsplash halo. It is interesting to note that this behaviour is peculiar to the CDM1/WDM1 set of hosts, but we consider it statistically insignificant.

3.6 Relative Velocities

So far we have compared and contrasted the spatial distribution and subhalos in the CDM and WDM models, and the degree to which these subhalos suffer mass loss. It is also of interest to ask whether the kinematics of subhalos in the respective models differs. We already learnt that the early infalling population in CDM1 is marginally faster than their counterpart in WDM1. Hence, if there are systematic differences between the models, what might the implication be for a system such as the “Bullet Cluster”? This is an extremely high velocity merger between two galaxy clusters (Milosavljević et al. 2007; Markevitch et al. 2002) and it has prompted discussion as to whether such high relative velocities (of order ~ 4500 km/sec) can be accommodated within the CDM model (Nusser 2007; Angus & McGaugh 2007; Springel & Farrar 2007; Hayashi & White 2006; Gill et al. 2005). We might expect such high relative velocities to be sensitive to the large scale gravitational

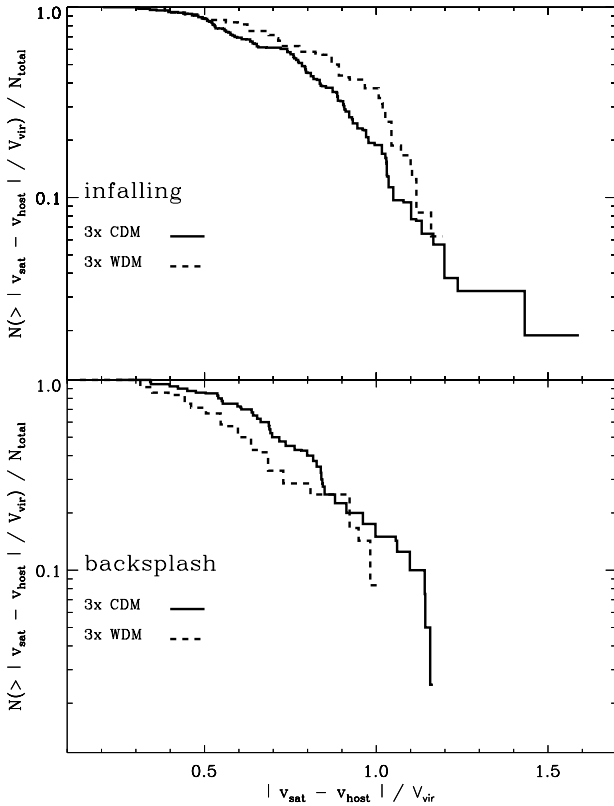


Figure 10. Same as Figure 9 but for the backsplash and infalling population, respectively.

field.³ Furthermore, if there are differences in the relative velocity distributions in the WDM and CDM models, this could also allow limits to be placed on the nature of the dark matter.

In Figure 9 we plot the cumulative distribution of relative velocities ($V_{\text{sat}} - V_{\text{host}}$) for all interior subhalos, where V_{sat} and V_{host} are the centre-of-mass velocities of all particles inside the virial radius of the subhalo and the host, respectively. Relative velocities have been normalised to the circular velocity V_{vir} of the host at the virial radius. If we compute this quantity for the “Bullet Cluster” using the estimate of the mass deduced from weak lensing (Clowe et al. 2004), the normalised collision speed ($(V_{\text{sat}} - V_{\text{host}})/V_{\text{vir}}$) is approximately 1.9 (and shown as a thin vertical line). This figure reveals that $\sim 6\%$ of subhalos in the CDM model have normalised relative velocities in excess of 1.9, compared to $\sim 10\%$ in the WDM model. In other words, the probability of a high-speed encounter is greater in the WDM model than in the CDM model.

We have computed the same distributions for infalling and backsplash (sub)halos and the results are shown in Figure 10. There we observe that the infalling population in the WDM model is marginally faster than its CDM counterpart. However, we also note that the fastest infalling satellite can always be found in the CDM

³ We caution the reader that the “Bullet” cluster is a system where the host (and the “Bullet” itself) is an order of magnitude more massive than the hosts (and satellites) presented in this study. While the existence of the “Bullet” cluster may serve as a motivation for the study of relative velocities any conclusions drawn from our results are to be extrapolated to the “Bullet” system with care. This is especially so because the differences between CDM and WDM are less prominent on scales corresponding to the “Bullet” cluster.

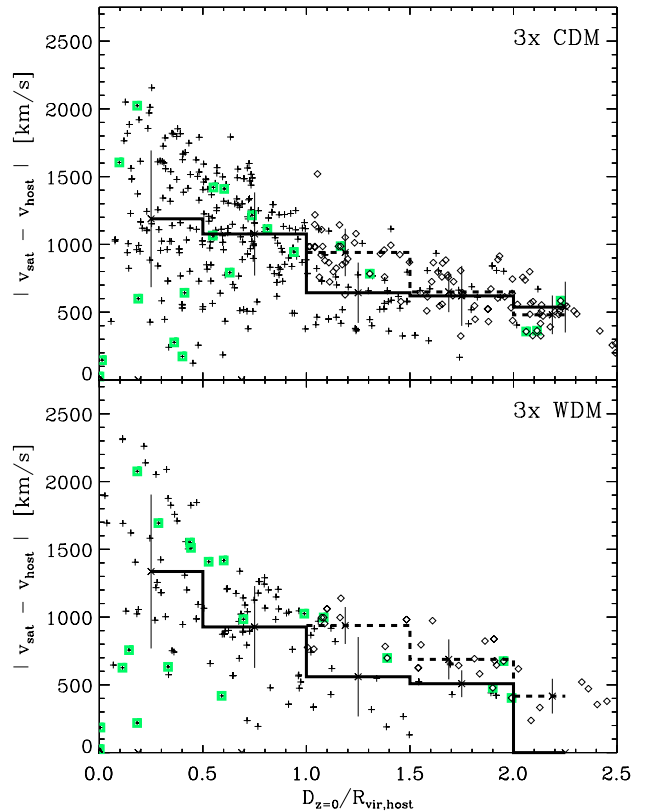


Figure 11. The absolute value of the relative velocities between the (sub)halos and their respective host versus their distance at the present time is shown. Diamonds represent the infalling population and black crosses denote the interior and backsplash populations. The thick solid lines are the mean values with error bars showing the standard deviation in each bin. For clarity, these are offset for the infalling halos. The squares denote the 20 most massive subhalos.

model. Or in other words, in WDM there are more infalling subhalos with relative velocities up to about $1.2 \times V_{\text{vir}}$, but in CDM there exists the odd satellite with a velocity as high as $\sim 1.5 \times V_{\text{vir}}$. One potential explanation of this may be that subhalos suffer “dynamical friction within the filaments”. As shown by Knebe et al. (2003), more mass in CDM filaments is found in gravitationally bound objects whereas the mass in a WDM filament is more uniformly distributed, which may lead to enhanced dynamical friction. Therefore, subhalos falling along filaments may have their infall velocities reduced and hence we a) do not find exceedingly fast subhalos and b) observe an increase in the number of objects in the range $0.75\text{--}1.2 V_{\text{vir}}$. The situation though is different for the backsplash population that appears to be slower than its CDM counterpart.

In Figure 11 we plot the (unnormalised) relative velocities of subhalos as a function of their present-day halocentric radii. Interior and backsplash populations are represented by crosses while infalling subhalos are represented by diamonds; we also highlight the 20 most massive subhalos by green squares.

There are a number of points to note in this figure. The first is that the subhalos with the highest relative velocities are concentrated towards the centre of the host, nestled in its potential well. The second is that the most massive subhalos (green squares) are not responsible for the high-velocity tail that we observe in Figure 9. The third point is that the WDM backsplash population a) does not

extend spatially as far out as for its CDM counterpart and b) has lower velocities leading to the observed steeper decline of the velocities with increasing clustercentric distance. The fourth and final point is that infalling subhalos are a distinct population kinematically, tending to have higher velocities than backsplash galaxies (see also Gill et al. 2005). We conclude that the kinematics of subhalos is unlikely to allow us to differentiate between the WDM and CDM models.

4 DISCUSSION & CONCLUSIONS

We have compared and contrasted the properties of subhalos orbiting in a set of simulated galaxy cluster hosts in the CDM and WDM models. The mass and force resolution of our simulations were sufficient to our host halos with $\sim 10^6$ particles within the virial radius at $z=0$, and we could follow the orbital evolution of hundreds of subhalos in detail using outputs finely spaced in time ($\Delta t \approx 170$ Myrs) from the formation time of the host to the present day.

Our study has revealed that many of the properties of subhalos in the CDM model and the WDM model we have studied are similar. Subhalos in both the CDM and WDM models are distributed anisotropically with respect to the major axis of their host, and the phenomenon of “backsplash” halos is common to both models. Other studies have shown that low-mass halos in WDM models tend to be less centrally concentrated than their counterparts in the CDM model (Colin et al. 2007), and this leads to enhanced mass loss via tidal stripping for subhalos in WDM models. We find no evidence for a well pronounced correlation between the age of a subhalo and its present day halocentric radius in either model. Interestingly, we find that subhalos in the WDM model are likely to have higher (infall) velocities than in the CDM model.

Our results nevertheless suggest that it is unlikely that the spatial distribution and kinematics of subhalos can be used to differentiate between the CDM and WDM models at $z=0$. It might be possible to detect differences at higher redshifts, when the effect of the filtering mass is more pronounced (e.g. Power et al. 2008). Furthermore, it might be possible to detect differences in the stellar populations and star formation histories of the satellite galaxies that are hosted by subhalos (e.g. Gao & Theuns 2007), which will be sensitive to the mass assembly histories of the (sub)halos. However, such measures depend explicitly on the veracity of galaxy formation modelling, and so it seems more likely that estimates of the small scale power spectrum deduced from the Lyman- α forest (e.g. Viel et al. 2007) may provide stronger constraints. Nevertheless, it is important to consider the various strands of observational evidence when piecing together the dark matter puzzle.

ACKNOWLEDGEMENTS

AK acknowledges funding through the Emmy Noether Programme by the DFG (KN 755/1). CP and BKG acknowledge the support of the Australian Research Council supported “Commonwealth Cosmology Initiative”⁴, grant DP 0665574. The simulations were carried out on the Swinburne Supercomputer at the Centre for Astrophysics & Supercomputing, Swinburne University. All of the analyses was carried out on the Sanssouci cluster at the AIP.

This paper has been typeset from a $\text{\TeX}/\text{\LaTeX}$ file prepared by the author.

REFERENCES

- Abazajian K., 2006, Phys. Rev. D, 73, 063513
 Agustsson I., Brainerd T. G., 2006, ApJ, 650, 550
 Agustsson I., Brainerd T. G., 2007, ArXiv e-prints, 704
 Angus G. W., McGaugh S. S., 2007, ArXiv e-prints, 704
 Avila-Reese V., Colín P., Valenzuela O., D’Onghia E., Firmani C., 2001, ApJ, 559, 516
 Bailin J., Power C., Norberg P., Zaritsky D., Gibson B. K., 2007, ArXiv e-prints, 706
 Balogh M. L., Navarro J. F., Morris S. L., 2000, ApJ, 540, 113
 Bardeen J. M., Bond J. R., Kaiser N., Szalay A. S., 1986, ApJ, 304, 15
 Bento M. C., Bertolami O., Rosenfeld R., Teodoro L., 2000, Phys. Rev. D, 62, 041302
 Bland-Hawthorn J., Peebles P. J. E., 2006, Science, 313, 311
 Bode P., Ostriker J. P., Turok N., 2001, ApJ, 556, 93
 Bullock J. S., 2001, ArXiv Astrophysics e-prints (0111005)
 Clowe D., Gonzalez A., Markevitch M., 2004, ApJ, 604, 596
 Colin P., Valenzuela O., Avila-Reese V., 2007, ArXiv e-prints, 709
 Dalcanton J. J., Hogan C. J., 2001, ApJ, 561, 35
 De Lucia G., Kauffmann G., Springel V., White S. D. M., Lanzoni B., Stoehr F., Tormen G., Yoshida N., 2004, MNRAS, 348, 333
 Diemand J., Kuhlen M., Madau P., 2007, ApJ, 667, 859
 Diemand J., Moore B., Stadel J., 2005, Nature, 433, 389
 Faltenbacher A., Li C., Mao S., van den Bosch F. C., Yang X., Jing Y. P., Pasquali A., Mo H. J., 2007, ApJ, 662, L71
 Gao L., Theuns T., 2007, Science, 317, 1527
 Gao L., White S. D. M., Jenkins A., Stoehr F., Springel V., 2004, MNRAS, 355, 819
 Gentile G., Tonini C., Salucci P., 2007, A&A, 467, 925
 Gill S. P. D., Knebe A., Gibson B. K., 2004, MNRAS, 351, 399
 Gill S. P. D., Knebe A., Gibson B. K., 2005, MNRAS, 356, 1327
 Gill S. P. D., Knebe A., Gibson B. K., Dopita M. A., 2004, MNRAS, 351, 410
 Goerdt T., Moore B., Read J. I., Stadel J., Zemp M., 2006, MNRAS, 368, 1073
 Hayashi E., White S. D. M., 2006, MNRAS, 370, L38
 Kang X., van den Bosch F. C., Yang X., Mao S., Mo H. J., Li C., Jing Y. P., 2007, MNRAS, 378, 1531
 Klypin A., Kravtsov A. V., Valenzuela O., Prada F., 1999, ApJ, 522, 82
 Knebe A., Devriendt J. E. G., Gibson B. K., Silk J., 2003, MNRAS, 345, 1285
 Knebe A., Devriendt J. E. G., Mahmood A., Silk J., 2002, MNRAS, 329, 813
 Knebe A., Gill S. P. D., Gibson B. K., Lewis G. F., Ibata R. A., Dopita M. A., 2004, ApJ, 603, 7
 Knebe A., Green A., Binney J., 2001, MNRAS, 325, 845
 Knebe A., Power C., Gill S. P. D., Gibson B. K., 2006, MNRAS, 368, 741
 Kravtsov A. V., Gnedin O. Y., Klypin A. A., 2004, ApJ, 609, 482
 Lacey C., Cole S., 1993, MNRAS, 262, 627
 Libeskind N. I., Cole S., Frenk C. S., Okamoto T., Jenkins A., 2007, MNRAS, 374, 16
 Libeskind N. I., Frenk C. S., Cole S., Helly J. C., Jenkins A., Navarro J. F., Power C., 2005, MNRAS, 363, 146
 Little B., Knebe A., Islam R. R., 2003, MNRAS, 341, 617

⁴ <http://www.theccci.org>

- Mamon G. A., Sanchis T., Salvador-Solé E., Solanes J. M., 2004, *A&A*, 414, 445
- Markevitch M., Gonzalez A. H., David L., Vikhlinin A., Murray S., Forman W., Jones C., Tucker W., 2002, *ApJ*, 567, L27
- McGaugh S. S., de Blok W. J. G., Schombert J. M., Kuzio de Naray R., Kim J. H., 2007, *ApJ*, 659, 149
- Milosavljević M., Koda J., Nagai D., Nakar E., Shapiro P. R., 2007, *ApJ*, 661, L131
- Moore B., Diemand J., Stadel J., 2004, in Diaferio A., ed., *IAU Colloq. 195: Outskirts of Galaxy Clusters: Intense Life in the Suburbs On the age-radius relation and orbital history of cluster galaxies*. pp 513–518
- Moore B., Ghigna S., Governato F., Lake G., Quinn T., Stadel J., Tozzi P., 1999, *ApJ*, 524, L19
- Navarro J. F., Hayashi E., Power C., Jenkins A. . R., Frenk C. S., White S. D. M., Springel V., Stadel J., Quinn T. R., 2004, *MNRAS*, 349, 1039
- Nusser A., 2007, *ArXiv e-prints*, 709
- Power C., Bland-Hawthorn J., Lewis G., 2008, in preparation, 0, 0
- Reed D., Governato F., Quinn T., Gardner J., Stadel J., Lake G., 2005, *MNRAS*, 359, 1537
- Reed D., Governato F., Verde L., Gardner J., Quinn T., Stadel J., Merritt D., Lake G., 2005, *MNRAS*, 357, 82
- Sales L. V., Navarro J. F., Abadi M. G., Steinmetz M., 2007, *MNRAS*, 379, 1464
- Seljak U., Zaldarriaga M., 1996, *ApJ*, 469, 437
- Shaw L. D., Weller J., Ostriker J. P., Bode P., 2007, *ApJ*, 659, 1082
- Spergel D. N., Steinhardt P. J., 2000, *Physical Review Letters*, 84, 3760
- Spergel D. N. e. a., 2007, *ApJS*, 170, 377
- Springel V., Farrar G. R., 2007, *MNRAS*, 380, 911
- Springel V., White S. D. M., Jenkins A., Frenk C. S., Yoshida N., Gao L., Navarro J., Thacker R., Croton D., Helly J., Peacock J. A., Cole S., Thomas P., Couchman H., Evrard A., Colberg J., Pearce F., 2005, *Nature*, 435, 629
- Tasitsiomi A., Kravtsov A. V., Gottlöber S., Klypin A. A., 2004, *ApJ*, 607, 125
- Tormen G., 1997, *MNRAS*, 290, 411
- Viel M., Becker G. D., Bolton J. S., Haehnelt M. G., Rauch M., Sargent W. L. W., 2007, *ArXiv e-prints*, 709
- Viel M., Lesgourgues J., Haehnelt M. G., Matarrese S., Riotto A., 2006, *Physical Review Letters*, 97, 071301
- Wang J., White S. D. M., 2007, *MNRAS*, 380, 93
- Warnick K., Knebe A., 2006, *MNRAS*, 369, 1253
- Warnick K., Knebe A., Power C., 2008, *MNRAS submitted*, 544
- Willman B., Governato F., Dalcanton J. J., Reed D., Quinn T., 2004, *MNRAS*, 353, 639
- Zentner A. R., Bullock J. S., 2003, *ApJ*, 598, 49
- Zentner A. R., Kravtsov A. V., Gnedin O. Y., Klypin A. A., 2005, *ApJ*, 629, 219